

An Evaluation of Carbon and Mixed Metal Oxide Electrodes for High Voltage Redox Flow Batteries

Joseph A. Murphy¹, Tyler Petek², and Jesse S Wainright^{3,*}

1 - School of Science, Waterford Institute of Technology, Waterford, Ireland

2 - De Nora Tech, LLC, 7590 Discovery Lane, Concord OH 44077

3 - Department of Chemical and Biomolecular Engineering
Case Western Reserve University
10900 Euclid Ave, Cleveland, OH 44106

Abstract

Aqueous redox flow battery (RFB) technology is limited by relatively low energy and power densities; thus, positive redox couples with higher thermodynamic potentials are of interest. However, higher voltage couples introduce additional complications related to electrode corrosion and the possibility of oxygen evolution as an un-wanted side reaction. In this effort, the stability and catalytic activity for typical carbon felt electrodes were determined for the positive reaction in common (Br^-/Br_2 , $\text{V}^{4+}/\text{V}^{5+}$) and higher voltage ($\text{Mn}^{2+}/\text{Mn}^{3+}$, $\text{Ce}^{3+}/\text{Ce}^{4+}$) RFB chemistries. Weight loss measurements were performed as a test of carbon oxidation and/or loss of material due to mechanical breakdown. In addition to baselining existing carbon electrodes, De Nora Tech, LLC provided several examples of DSA® anodes¹, their mixed metal oxide (MMO) coated titanium electrodes, to be evaluated in similar tests to provide a comparison of performance. The MMO electrodes provided similar or higher catalytic activity and were immune to corrosion. While some MMO formulations also exhibited higher activity for oxygen evolution, a formulation based on iridium and tantalum oxides was found to have similar activity for the oxygen evolution reaction (OER) as graphite.

*- corresponding author, ORCID 0000-0001-7902-7238
e: jsw7@case.edu, ph: 216-368-5382

Keywords: flow battery, carbon, mixed metal oxide, degradation

¹ DSA® is a registered trademark of Industrie De Nora S.p.A in Europe, USA and other countries. De Nora owns more than 355 patent application families worldwide.

1. Introduction

Redox flow batteries (RFBs) are a promising technology for efficient energy storage and grid stabilization[1,2]. There are many examples of RFBs, some of the most common being all-vanadium redox flow battery (VRB), iron-chromium flow battery (ICB) and zinc-bromine flow battery (ZnBr). Other redox chemistries such as S_2^{2-}/S_4^{2-} [3,4], Fe^{2+}/Fe^{3+} [5-8], Br^{3-}/Br^- [4,9-11], Ce^{3+}/Ce^{4+} [12,13] and Mn^{3+}/Mn^{2+} [3,14,15] have also been studied. In order for RFBs to compete with commercially available lithium ion alternatives [16, 17], they must be efficient and cost effective. Cost effectiveness can be achieved by choosing durable, in-expensive materials for the battery, such as carbon based electrodes. One of the most widely used materials is carbon felt[18-20]. Carbon electrodes have also been coated with metals such as iridium[21], doped with nitrogen[22] or decorated with nanomaterials such as graphene nanowalls[23] or graphite carbon nanotubes[24] to improve their catalytic activity. Recently, Zhou et al. reported activation of carbon papers and carbon cloth by heat-treatment and subsequent etching with KOH.[25] Bourke et al. also reported similar improvements using chemical pre-treatment of the carbon electrodes[26,27], whereas others have taken a thermal treatment approach[28-30].

Most of these surface treatment methods introduce functional groups onto the carbon electrode surface. This not only increases wettability of the carbon felt, but also the redox activity, attributed to the increased concentration of surface-active oxygen functional groups[26,27,31]. Heat treatment of carbon materials is still regarded as the best approach to incorporate oxygen containing groups onto their surfaces. Previous work carried out by our group showed that the introduction of oxygen containing functionalities enhances the kinetics of V^{2+}/V^{3+} but inhibits the kinetics of VO^{2+}/VO_2^+ [27,32]. In a separate study carried out by Fink et al.[31], the role of oxygen functional groups on electrode performance were also studied on pristine and heat-treated Rayon based carbon felt and a polyacrylonitrile (PAN) based carbon felt. Similar to our previous work, they found that the normalized rate constant for the V^{2+}/V^{3+} redox reaction increased with increasing number of oxygen functional groups, while the rate constant for VO^{2+}/VO_2^+ redox reaction decreased for both types of carbon felt electrodes.

All these studies, and many others in the community, have led to improvement of the electrochemical activity of various carbon materials. Performance of RFBs has increased as a direct result. However, despite these improvements, the lifetime of these carbon materials is not widely reported. The use of heat treated carbon materials such as PAN based carbon papers SGL 10 AA[33], or Rayon based carbon felt SGL GFA6[34], resulted in an initial performance increase in the VRB. However, in both cases, the cycling stability was found to be very poor, with the electrodes losing their initial activity after a number of cycles. The bipolar carbon plates in a vanadium redox flow battery have also been shown to hinder lifetime in studies where anodic potentials exceeded 2.0 V resulting in cracks and bulging of the anodic plate[35]. Similarly, studies carried out using galvanostatic charging in similar systems reported damage to anodic carbon bipolar plates, with little effect noted on the cathodic plates despite large quantities of hydrogen evolution[36]. Thus it has been shown that carbon as a material in vanadium redox flow batteries is not an ideal material where lifetime is a requirement.

In this study, the performance of a typical commercial carbon felt after heat-treatment was investigated in a number of different chemistries used in traditional RFBs, including the most widely reported VRB system. Stability of the carbon felt was investigated over an extended period of time (>200 hrs). The materials were characterized by weight measurement,

electrochemical impedance spectroscopy (EIS), polarization data and in some cases scanning electron microscopy (SEM) before and after cycling. Alternative mixed metal oxide coated titanium electrode materials, DSA®, provided by De Nora Tech, LLC were also investigated and compared to the carbon felt electrode. A cost model was also developed to provide an initial estimate of the commercial potential for these alternative electrodes in RFB systems.

2. Experimental

2.1 Electrode materials and preparation

Carbon felt electrodes were tested in each electrolyte. The felt was Morgan Advanced Materials' VDG grade, 1/8" (3.2 mm) nominal thickness. This is a 'graphitic' felt, which is produced by pyrolysis of a rayon precursor at 1900°C. The felts were heat treated before use to improve their wettability; the heat treatment consisted of being held at 400°C in air for 6 hours. Each sample was cut from the same roll of VDG material.

Six DSA® electrodes with different compositions (see below) were provided by De Nora Tech, LLC. In each case the mixed metal oxide coating was applied to a titanium substrate. These electrodes were tested as received. Each electrode composition is commercially available from De Nora Tech, LLC for other industries and no attempt was made to optimize these formulations for this application.

2.2 RFB cell design and electrolyte preparation

Typical RFB cells (See Fig. 1) with membrane areas of either 3 or 6 cm² were used in this study. In some cases, identical trials were run in both cells, with similar results. In each case, a single electrolyte tank fed both the positive and negative side of the battery, with the return lines coupled together and connected back to the same electrolyte tank.

Rounded rectangular carbon felt electrodes were cut from larger sheets of carbon felt via a dye cut. Rubber gasketing of 2.4-2.5 mm thickness was cut using a similar dye cut from sheets of Viton rubber to create the electrolyte channel on both the positive and negative side of the battery. The thickness of the gasketing is thus 75-80% of the thickness of the uncompressed carbon felt. Compression of the felt allowed electrical contact to be maintained with the graphite current collector.

The felt electrodes were weighed to ±0.1 mg before and after each trial. The final weight was taken after copious rinsing of the electrodes with de-ionized water and drying to a constant weight. Most of the test cells used Nafion 117 as a separator; in a few instances Nafion 212 was used.

For flow battery tests, the vanadium electrolyte consisted of 0.5M VOSO₄ and 0.5M V₂O₅ in 4M H₂SO₄. A mixed vanadium manganese electrolyte was made by adding 0.5M MnSO₄ with 0.5M V₂O₅ in 4 M H₂SO₄. The bromine electrolyte consisted of 0.1M Br₂ in 1M HBr. Under these conditions, the Br₂ is completely soluble as Br₃⁻ and the electrolyte is a single liquid phase. The cerium electrolyte was 0.1M Ce³⁺ with 0.1M Fe³⁺ in 3M methane sulfonic acid (MSA) as a supporting electrolyte. The cerium salt used was cerium carbonate and the iron salt was iron sulfate. The cerium carbonate was first dissolved in 70% MSA, which was then diluted to 3M and the iron sulfate was added at the end. It should be noted that contrary to the literature, even at 0.1M the cerium was not completely dissolved and the actual concentration during testing was somewhat lower.

For cyclic voltammetry tests to determine the redox activity of the various electrodes, the cerium electrolyte consisted of 0.1M Ce³⁺ only, without any Fe³⁺, in 3M methane sulfonic acid. Similarly, the manganese electrolyte for CV tests consisted of 0.5M MnSO₄ in sulphuric acid, without any vanadium. In both of these cases, at least 10 cycles were performed to generate the oxidized species (Ce⁴⁺ or Mn³⁺) in solution and obtain a steady voltammogram.

2.3 Carbon Based Electrode Testing

For each redox couple the following electrochemical measurements were made:

- Polarization curves (initial, final and at intermediate times)
- AC impedance (initial, final and intermediate)
- Polarization at a fixed current density during the test

The details of how each cell was operated are given below in the discussion for each different electrolyte. In general, the current density applied was varied, depending on the activity of each electrode/redox couple, to give a total cell polarization on the order of 200 mV at the start of the test. The symmetric nature of the design provided a constant reactant composition throughout each test. All electrochemical experiments were performed at room temperature (20°C).

2.4 DSA® Electrode Testing

Three electrode (beaker cell) tests were performed at room temperature (20°C) using Pt gauze counter electrodes and silver/silver chloride (Ag/AgCl) reference electrodes. The electrolytes were not stirred. In most cases, two repeat measurements were made for each combination of electrode formulation and electrolyte. The electrochemical measurements performed included cyclic voltammetry over a wide potential range (+0.25V to +1.5V vs Ag/AgCl), and then over two narrower potential ranges (-300mV to +300 mV, and -30mV to +30 mV, with respect to the expected reversible potential for the redox couple present). The wider potential scans were performed at 25 mV/s, while the ± 30 mV scans were performed at 2 mV/s to minimize capacitive charging currents. AC impedance spectroscopy was also performed at the reversible potential, with a 10 mV AC amplitude, over a frequency range from 20,000 Hz to 0.2 Hz.

The kinetic activity of each electrode/electrolyte combination was estimated from the ±30 mV scans in conjunction with the AC impedance results. The solution resistance was obtained from the AC impedance at high frequency. This value was used to correct the polarization observed in the voltammetry for the voltage loss in solution. The ±30 mV scans were assumed to be in the linear polarization region and that the mass transfer resistance (R_{mt}) was negligible, such that the slope (voltage over current) after IR correction represented the charge transfer resistance (R_{ct}). The charge transfer resistance was then used to calculate the exchange current ($I_0 = RT/nFR_{ct}$). The exchange current was then used to calculate the apparent exchange current density, based on the geometric area of the electrode, ($i_0 = I_0/\text{area}$). The true exchange current density, which would be based on the electrochemically active surface area, could not be determined since the DSA® electrodes were on Ti substrates and the surface roughness after coating is not known. However, as the electrode coating is non-porous, the roughness factor should be low and similar to the graphite rod used for comparison. Also, as the roughness should be consistent between different formulations, comparisons based on the apparent exchange current density based on the geometric area should be reasonable.

Rates of oxygen evolution were estimated for DSA® electrodes and for a graphite rod as a stand-in for the carbon felt. In each case, cyclic voltammetry was used to measure the current at a given potential for electrolytes with and without the redox couples present in the electrolyte. By comparing the current at a higher potential to the baseline obtained at lower potential (in the absence of the redox couple) an estimate of the oxygen evolution current was obtained. For example, for the manganese system the current at 1.0V vs Ag/AgCl was taken as a baseline, this current is the non-Faradiac (capacitive) current present at all potentials. This current is the same in the neat acid electrolyte and in the electrolyte with Mn²⁺ present. Then the current was determined from the voltammetry in both electrolytes at +1.3V vs Ag/AgCl. This potential represents an overpotential of 50 mV for the Mn²⁺→Mn³⁺ reaction, which represents a reasonable operating overpotential in an actual redox flow battery. The coulombic efficiency is then calculated using equation 1. The procedure is shown graphically in Fig 2. A values were taken from the scan going to more positive potentials. Any in-efficiency is assumed to be the result of oxygen evolution.

$$C.E. = 100 * \left\{ 1 - \left[\frac{\text{current at 1.3V} - \text{current at 1.0V in neat acid}}{\text{current at 1.3V} - \text{current at 1.0V in acid plus Mn}} \right] \right\} \quad [1]$$

3. Results and Discussion

3.1 Carbon Felt

The first test performed evaluated the mechanical integrity of the felt under flowing conditions. A cell was assembled, and de-ionized water was circulated through the cell using the same flow rate as was used in subsequent tests with a redox couple present. Weight loss measurements before and after one week showed no weight loss. In fact, a small weight gain was observed (about 2% of the initial electrode weight), suggesting that the reproducibility of the weighing and drying process is on that order, and that a weight gain or loss of at least 4% is the minimum that can be considered statistically significant. It should be noted that other felt materials from other manufacturers have been previously tested in this manner and have shown significant weight loss due to mechanical degradation induced by the flowing liquid, with many fine particles being released from the felt. However, the Morgan VDG material appeared to be immune to this degradation. Thus, in subsequent tests with the various redox couples, it is very likely that any weight loss is due to chemical, not mechanical, degradation.

3.1.1 V^{4+/5+} Redox Couple, E₀ = 1.0V vs NHE

The stability of the carbon felt electrode in conjunction with the V^{4+/5+} redox couple was also evaluated in a symmetric configuration. The polarization vs time behaviour for three separate trials is shown in Figure 3. For these sets of experiments, each cell was polarized galvanostatically at slightly different current densities and monitored over the course of roughly 10 days. Measurements of electrode masses before and after use were also recorded and are shown in Table 1. It is apparent that after about 200 hrs of operation, the cell potential undergoes a significant increase in value in each trial, which we attribute to degradation of the electrodes. No color change was observed in the electrolyte solution throughout the testing, which suggests that the V^{4+/5+} solution remained unaltered from start to finish.

The results from the EIS scans are shown in Fig 4. A scan prior to operation (labelled initial EIS in each case) and after each cell had been operated for several days (labelled as final EIS)

were performed. It can be seen that a clear shift in high frequency resistance was measured in all three cases. Similarly, the charge transfer loop has increased with time. This increase in resistance correlated with the increase in polarization, both being a good indication that the electrode material has suffered some damage. The electrode mass before and after shows that both the positive and negative electrodes suffered loss of material, the greater loss occurring on the positive electrode, while the negative electrode loss must be considered within the error of the measurement. Since it is considered unlikely that the Nafion membrane was significantly altered during the experiment, the change in the high frequency resistance is most likely associated with an increased contact resistance, likely between the positive felt and its current collector.

SEM images were recorded of the electrode materials before and after use. Examples of these images are shown in Fig 5. The first micrograph, 5(A), shows a typical group of carbon fibres interwoven to make up the 1/8" thick electrode material as received. The individual fibres themselves are in the region of 15-20 μm thick, with a large void fraction between them. Fig 5(B) shows a similar electrode after being heat treated and used in a mechanical only experiment with water running through the system for approximately 200 hours. Very little difference is noted between both the images seen in 5(A) and 5(B). This corresponds to a negligible loss of electrode material recorded before and after the experiment had run. The image of the fibres in 5(C) shows sign of damage, after it had been run in a V^4/V^5 symmetric cell for in excess of 200 hours. This would support the mass loss measurements recorded post battery charge. Similarly, damage was noted to have occurred to the negative electrode, as shown in Fig 5 (D), however the extent of the damage is somewhat lessened as was noted in the loss of mass measurements.

3.1.2 $\text{Br}^- / \text{Br}_3^-$ Redox Couple, $E_0 = 1.06\text{V}$ vs NHE

The stability of the carbon felt electrode in conjunction with the $\text{Br}^- / \text{Br}_3^-$ redox couple was evaluated in a symmetric cell as shown in Fig 1. Similar to previous experiments, a constant current was applied, and the resulting cell potential was measured at intervals from start to finish. The resulting polarization vs time behavior is shown in Fig 6.

A constant current density of 200 mA/cm^2 was applied to the bromine cell for a duration of approximately 120 hours (or 5 days). An increase in potential was measured from the onset, doubling within about 50 hours on test and increasing more slowly at longer times. AC impedance scans (not shown) taken before and after the constant current polarization indicated an increase in both the high frequency and charge transfer resistances.

A mass loss of 7% wt and 2.4% wt were measured in the positive and negative electrodes respectively. Again, the weight change for the negative electrode is within the error of the measurement. Also, corrosion of the positive current collector was noted to have occurred, with the entire region underneath the electrode uniformly etched to a depth of several hundred microns.

3.1.3 $\text{Mn}^{2+/3+}$ Redox Couple, $E_0 = 1.4\text{V}$ vs NHE

The stability of the carbon felt electrode in conjunction with the $\text{Mn}^{2+/3+}$ redox couple was evaluated in an asymmetric, single tank configuration. The electrolyte was 0.5M Mn^{2+} with 0.5M V^{5+} in 4 M H_2SO_4 as a supporting electrolyte. In the asymmetric configuration, the positive electrode oxidizes Mn^{2+} to Mn^{3+} , while the negative electrode reduces V^{5+} to V^{4+} .

Both reactant streams are returned to the single tank, where the Mn^{3+} and V^{4+} react in solution to reverse the electrochemical reactions and maintain a constant electrolyte composition. This test method was used since a soluble Mn^{3+} salt is not readily available. This method also minimizes the concentration of Mn^{3+} in the electrolyte, limiting the formation of insoluble MnO_2 which can be formed by the disproportionation of Mn^{3+} to Mn^{2+} and Mn^{4+} . [38]

The battery was operated at a constant current density of 43 mA/cm^2 , and allowed to run for more than 250 hours. The lower current density (as compared to the $\text{V}^{4+/5+}$ and $\text{Br}^{-/3-}$ cells) was necessitated by the relatively sluggish $\text{Mn}^{2+/3+}$ kinetics. The cell potential was recorded and the resulting polarization vs time behavior is shown in Fig 7. Initially, the cell potential remained quite stable, showing only a slight increase after ~ 200 hours of operation. Between 200 and 260 hours of operation, the cell potential rapidly increased, reaching 667 mV at 260 hours. Gas bubbles were coming from the positive side of the cell during this time, with an increase in size and frequency of the gas evolution as the cell was operating. At 260.5 hours, the potential had reached a peak value of 752 mV and the test was terminated. The gas evolution at this stage was noted to be extremely higher than observed previously.

From EIS scans it can be seen that the high frequency and charge transfer resistances have increased as a result of the cell operation as shown in Figure 8. The increase in the high frequency resistance is again likely to be due to an increase in contact resistance due to electrode degradation. After disassembly, the positive electrode was found to have lost 15.1% of its original mass, while the negative electrode lost 2.9%. Furthermore, the graphite current collector on the positive side of the cell had also experienced corrosion, similar to what was observed in the bromine cell.

Given the visible gas evolution at the positive electrode, the complete failure of the cell after 250 hours can be attributed to a lack of V^{5+} in the electrolyte. As oxygen is evolved (instead of the formation of Mn^{3+}), the lack of Mn^{3+} returning to the reservoir results in a build-up of V^{4+} and a deficit of V^{5+} . The reservoir volume was 125 ml and was initially 0.5M V^{5+} , equivalent to 1.675 Ah. The total charge passed over 250 hours is equivalent to 32.25 Ah. This suggests that $\approx 5\%$ of the total current went to oxygen evolution.

3.1.4 $\text{Ce}^{3+/4+}$ Redox Couple, $E_0 \approx +1.625\text{V}$ vs NHE

The stability of the carbon felt electrode in conjunction with the $\text{Ce}^{3+/4+}$ redox couple was evaluated in an asymmetric, single tank configuration. In the asymmetric configuration used, the positive electrode oxidized Ce^{3+} to Ce^{4+} , while the negative electrode reduced Fe^{3+} to Fe^{2+} . Both reactant streams are returned to a common reservoir, where the Ce^{4+} and Fe^{2+} chemically reacted in solution to reverse the electrochemical reactions and maintain a constant electrolyte composition. This test method was used since a soluble Ce^{4+} salt is not readily available.

Four separate trials of the Ce/Fe cell were carried out. In each trial, it was found to be necessary to hold the cell at a constant voltage as opposed to a constant current. Under constant current conditions, the cell potential was initially about 1.0V, consistent with the desired reactions of $\text{Ce}^{3+} \rightarrow \text{Ce}^{4+}$ on the positive electrode and $\text{Fe}^{3+} \rightarrow \text{Fe}^{2+}$ on the negative electrode, based on literature reports for the potential of the $\text{Ce}^{3+/4+}$ reaction in MSA [39]. However, fairly quickly the cell potential at a constant current would drop to a much lower value. Our analysis of this change in the potential (which was confirmed by the subsequent constant voltage trials) is that oxygen evolution was occurring at the positive electrode, as well as cerium oxidation. Bubbles of gas could be seen in the electrolyte leaving the positive compartment of the cell. Since the

oxygen evolved left the system (the reservoir was not sealed), Fe^{2+} eventually built up in the electrolyte, since there wasn't an equal amount of Ce^{4+} available to react with it. As the Fe^{2+} concentration in the electrolyte increased, the positive reaction could switch to $\text{Fe}^{2+} \rightarrow \text{Fe}^{3+}$, which occurs at a much lower potential than cerium oxidation and thus the cell potential dropped. This effect could also be seen in the polarization curves taken at various points during the constant potential tests, as shown in Figure 9. In this Figure, we would expect essentially no current at cell potentials less than 0.8V as shown in the initial curve. However, a significant current at potentials less than 0.8V can be observed after just one day on test. This current arises from the oxidation of Fe^{2+} at the positive electrode as it built up in the electrolyte in proportion to the amount of oxygen evolved.

In each of the four trials with Ce, the mass of the positive electrode was unchanged within experimental error. This is a somewhat surprising result given that the lower voltage Mn and Br systems showed definitive carbon corrosion. However, we know that the oxidation current throughout the test is a mixture of Fe and Ce oxidation and oxygen evolution, so it's unclear what would happen if the positive electrode was oxidizing Ce^{3+} solely.

3.2 DSA® Electrodes

In this section, we present the results for the exchange current densities for the various positive redox couples on each of the DSA® electrode materials, and compare them to graphite. The components present in the six different DSA® electrodes provided by De Nora are given in Table 2 below.

The apparent exchange current densities for the various combinations of electrode and redox couple are shown in Fig 10. From the results shown in Fig 10 several conclusions can be made. The DSA® electrodes in general show the greatest activity for the Br^-/Br_2 reaction, particularly the 'D' formulation which contains Pt. The next highest exchange current for each formulation is for the $\text{V}^{4+/5+}$ reaction, while the $\text{Mn}^{2+/3+}$ reaction is generally the slowest. In each electrolyte, the DSA® electrodes show similar or greater kinetic activity than the graphite electrode (which was used to represent the graphitic felt electrodes discussed previously but with a similar form and surface area as the DSA® electrodes). Comparing the different DSA® formulations for $\text{V}^{4+/5+}$ and Br^-/Br_2 , the highest activity was found with 'D', followed by 'C' and 'E' which are similar, then the 'A', 'B' and 'F' were generally the poorest performers. For the $\text{Mn}^{2+/3+}$ redox couple, formulation 'F' has the highest activity while formulations 'B' through 'E' all still demonstrated significantly better activity than graphite. It should be noted that Fig 10 does not include any results for the Ce redox couple. In the Ce electrolyte, oxygen evolution was the predominate reaction on all of the DSA® electrodes, and the activity for the Ce redox could not be determined.

When working with high potential redox couples ($>1\text{V}$ vs NHE), oxygen evolution must be avoided so that the coulombic efficiency is sufficiently high during charging. For the vanadium and bromine electrolytes, the redox potential is sufficiently low such that oxygen evolution is not a major concern. Using the cyclic voltammetry method described above, coulombic efficiencies of essentially 100% were obtained with each of the DSA® electrodes in both the vanadium and bromine electrolytes. Given the level of noise present, we estimate that the inefficiency must be greater than 2% to be reliably detected. However, for the manganese and cerium electrolytes, significant amounts of oxygen evolution occurred with each electrode

formulation. The results for the manganese electrolyte are shown in Table 3. The 'E' formulation was clearly superior in this instance, with only about 5% of the total current going to oxygen evolution, similar to that observed with a graphite electrode in the same potential range. It should be noted that for the graphite electrode, the in-efficiency could be a combination of oxygen evolution or carbon corrosion. With the DSA® electrodes, the in-efficiency is thought to be entirely oxygen evolution.

Greater amounts of oxygen evolution were observed for the cerium electrolyte where the redox potential is the highest of the chemistries evaluated. For all of the DSA® electrodes tested, oxygen evolution in the cerium electrolyte is >90% of the total current based on cyclic voltammetry (using a similar method as that used for the Mn electrolyte). Thus, for Ce redox, a stable electrode that is also highly in-active for oxygen evolution would need to be developed.

A few general conclusions can be drawn from the results obtained for the kinetic activity and oxygen evolution rates. Electrode D, which is the only formulation that includes platinum, gave the highest redox activity, and would appear to be preferable in the vanadium and bromine electrolytes. However, this formulation also resulted in significant amounts of oxygen evolution in the manganese electrolyte. Electrodes A and F, which contain Ir (which is often used as an oxygen evolution catalyst), not surprisingly also showed high rates of oxygen evolution in the manganese electrolyte. In contrast, electrode E, which also contains Ir but in conjunction with Ta, generated relatively little oxygen in the manganese electrolyte, about 5%, on par with the graphite electrode. For the DSA® electrodes based on Ru, not Ir, in-efficiencies on the order of 10-15% were observed in the manganese electrolyte, consistent with the fact that ruthenium oxide is generally considered a poorer O₂ evolution catalyst than platinum or iridium oxides. However, even this level of coulombic in-efficiency is too high for an effective flow battery system. Therefore, of these six 'off the shelf' possibilities, the E formulation would be preferred for a battery incorporating the Mn^{2+/3+} couple.

4. Conclusions

In this work, carbon electrode degradation as a result of cell operation was evaluated for four positive redox flow battery chemistries. All of the tests were carried so as to maintain constant concentrations of the oxidized and reduced species. In the vanadium cell (V^{4+/5+}), the carbon electrodes experienced some degradation as a result of operation. A large increase in cell potential was noted to occur after a time period of about 250 hours was reached, which we attribute primarily to a loss of material on the positive electrode. SEM micrographs of the electrode surfaces also showed signs of degradation when comparing to carbon electrodes that had not experienced charging in the vanadium cell. The bromine system experienced similar loss of electrode mass, but in about half the time (120 hrs) of that of the vanadium cell. Corrosion of the graphite positive current collector was also evident after the test. Lastly, charging in a manganese electrolyte also heavily damaged the carbon felt electrodes, with a 15.1% mass loss of the positive electrode measured. Increases in both high frequency and charge transfer resistances were identified using EIS, coinciding with degradation of the carbon electrodes. Corrosion of the positive current collector in the Mn cell was also noted to have occurred.

De Nora DSA® electrodes were evaluated as alternatives to carbon based electrodes. The kinetic behavior of 6 different formulations of DSA® electrodes were evaluated in $\text{Mn}^{2+/3+}$, $\text{V}^{4+/5+}$ and Br/Br_2 electrolytes using a 3-electrode assembly. Kinetic activity similar to that of a graphite electrode was observed in both the Mn^{2+} and $\text{V}^{4+/5+}$ electrolytes, with significantly faster kinetics seen with DSA® anodes in the Br/Br_2 based electrolyte. Coulombic efficiencies were calculated for all DSA® electrodes. A DSA® electrode based on Ir and Ta showed comparable efficiency ($\approx 95\%$) to that of graphite in the Mn electrolyte. However, three other formulations (A, D, F) evolved considerably amounts of oxygen in addition to oxidizing Mn^{2+} . With a $\text{Ce}^{3+/4+}$ electrolyte, oxygen evolution was the dominant reaction with all DSA formulations. None of the six formulations tested showed signs of corrosion as a result of experiments carried out in vanadium, manganese, or bromine electrolytes. Lastly, a cost model based on a 50 cell stack was developed to show a capital cost of \$150 / kWh is feasible with an DSA® positive electrode, if a lower cost electrolyte is used.

Acknowledgements / Conflict of Interest Statement

This work was funded in full by De Nora, LLC. One of us (JSW) has also received funding for other projects from De Nora LLC.

References

- [1] G. Kear, A. A. Shah, F.C. Walsh, Development of the all-vanadium redox flow battery for energy storage: a review of technological, financial and policy aspects, *Int. J. Energy Res.*, 36, (2012) 1105-1120.
- [2] A.Z. Weber, M.M. Mench, J.P. Meyers, P.N. Ross, J.T. Gostick, Q. Liu, Redox flow batteries: A review, *J. Appl. Electrochem.*, 41, (2011) 1137-1164.
- [3] W. Wang, L. Quo, L. Bin, W. Xiaoliang, L. Liyu, Y. Zhenguo, Recent Progress in Redox Flow Battery Research and Development, *Adv. Funct. Mater.*, 23, (2013) 970–986.
- [4] P. Zhao, H. Zhang, H. Zhou, B. Yi, Nickel foam and carbon felt applications for sodium polysulfide/bromine redox flow battery electrodes, *Electrochim. Acta*, 51, (2005) 1091-1098.
- [5] M.H. Chakrabarti, R.A.W. Dryfe, E.P.L. Roberts, Evaluation of electrolytes for redox flow battery applications, *Electrochim. Acta*, 52, (2007) 2189-2195.
- [6] Y.H. Wen, H.M. Zhang, P. Qian, H.T. Zhou, P. Zhao, B.L. Yi, Y.S. Yang, A study of the Fe(III)/Fe(II)–triethanolamine complex redox couple for redox flow battery application, *Electrochim. Acta*, 51, (2006) 3769-3775.
- [7] K.L. Hawthorne, T. J. Petek, M.A. Miller, J.S. Wainright, R. F. Savinell, An investigation into factors affecting the iron plating reaction for an all-iron flow battery, *J. Electrochem. Soc.*, 162, (2015) A108-A113.
- [8] T.J. Petek, N.C. Hoyt, J.S. Wainright, R.F. Savinell, Characterizing Slurry Electrodes Using Electrochemical Impedance Spectroscopy, *J. Electrochem. Soc.*, 163, (2016) A5001-A5009.
- [9] C. Ponce De Leon, A. Frias-Ferrer, J Gonzalez-Garcia, D.A. Szanto, F.C. Walsh, Redox flow cells for energy conversion, *J. Power Sources*, 160, (2006) 716-732.
- [10] Y. H. Wen, H. M. Zhang, P. Qian, H.T. Zhou, P. Zhao, B. L. Yi, Y. S. Yang, Studies on Iron ($\text{Fe}^{3+}/\text{Fe}^{2+}$) -Complex/Bromine (Br^2/Br^-) Redox Flow Cell in Sodium Acetate Solution, *J. Electrochem. Soc.*, 153, 5, (2006) A929-A934.
- [11] S.H. Ge, B.L. Yi, H.M. Zhang, Study of a high power density sodium polysulfide/bromine energy storage cell, *J. Appl. Electrochem.*, 34, (2004) 181-185.
- [12] B. Fang, S. Iwasa, Y. Wei, T. Arai, M. Kumagai, A study of the Ce(III)/Ce(IV) redox couple for redox flow battery application, *Electrochim. Acta*, 47, (2002) 3971-3976.
- [13] F. Xiong, D. Zhou, Z. Xie, Y. Chen, A study of the $\text{Ce}^{3+}/\text{Ce}^{4+}$ redox couple in sulfamic acid for redox battery application, *Appl. Energy*, 99, (2012) 291-296.
- [14] F.Q. Xue, Y.L. Wang, W.H. Wang, X.D. Wang, Investigation on the electrode process of the Mn(II)/Mn(III) couple in redox flow battery, *Electrochim. Acta*, 53, (2008) 6636–6642.
- [15] A.E.S Sleightholme, A.A Shinkle, Q. Liu, Y. Li, C.W. Monroe, L.T. Thompson, Non-aqueous manganese acetylacetonate electrolyte for redox flow batteries, *J. Power Sources*, 196, 13, (2011) 5742-5745.
- [16] B.A. Johnson, R.E. White, Characterization of Commercially Available Lithium-Ion Batteries, *J. Power Sources*, 70, 1, (1998) 48-54.
- [17] B. Dunn, H. Kamath, J.M. Tarascon, Electrical energy storage for the grid: a battery of choices, *Science*, 334, (2011) 928-935.
- [18] Z.R. Yeu, W. Jiang, L. Wang, S.D. Gardner, J.C.U. Pittman, Surface characterization of electrochemically oxidized carbon fibers, *Carbon*, 37 (1999) 1785-1796.
- [19] K. J. Kim, M.S. Park, Y.J Kim, J.H. Kim, S.X Doub, M.S. Kazacos, A technology review of electrodes and reaction mechanisms in vanadium redox flow batteries, *J. Mater. Chem. A*, 3, (2015) 16913-16933.

- [20] S.K. Park, J.M. Shim, J.H. Yang, C.S. Jin, B.S Lee, Y.S Lee, K.H Shin, J.D Jeon, The influence of compressed carbon felt electrodes on the performance of a vanadium redox flow battery, *Electrochim. Acta*, 116, (2014) 447-452.
- [21] W.H. Wang, X. D. Wang, Investigation of Ir-modified carbon felt as the positive electrode of an all-vanadium redox flow battery, *Electrochim. Acta*, 52, (2007) 6755-6762.
- [22] Y. Shao, X. Wang, M. Engelhard, C. Wang, S. Dai, J. Liu, Z. Yang, Y. Lin, Nitrogen-doped mesoporous carbon for energy storage in vanadium redox flow batteries, *J. Power Sources*, 195, (2010) 4375-4379.
- [23] W. Li, Z. Zhang, Y. Tang, H. Bian, T.W. Ng, W. Zhang, C.S. Lee, Graphene-Nanowall-Decorated Carbon Felt with Excellent Electrochemical Activity Toward $\text{VO}_2^+/\text{VO}^{2+}$ Couple for All Vanadium Redox Flow Battery, *Adv. Sci.*, 3, (2016) 1500276.
- [24] H.Q. Zhu, Y.M. Zhang, L. Yue, W.S. Li, G.L. Li, D. Shu, H.Y. Chen, Graphite-carbon nanotube composite electrodes for all vanadium redox flow battery, *J. Power Sources*, 184, (2008) 637-640.
- [25] X.L Zhou, T.S. Zhao, Y.K Zeng, L. An, L. Wei, A highly permeable and enhanced surface area carbon-cloth electrode for vanadium redox flow batteries, *J. Power Sources*, 329, (2016) 247-254.
- [26] A. Bourke, M. A. Miller, R. P. Lynch, X. Gao, J. Landon, J. S. Wainright, R. F. Savinell, D. N. Buckley, Electrode Kinetics of Vanadium Flow Batteries: Contrasting Responses of $\text{V}^{\text{II}}-\text{V}^{\text{III}}$ and $\text{V}^{\text{IV}}-\text{V}^{\text{V}}$ to Electrochemical Pretreatment of Carbon, *J. Electrochem. Soc.*, 163, (2016) A5097-A5105.
- [27] A. Bourke, M. A. Miller, R. P. Lynch, J. S. Wainright, R. F. Savinell, D. N. Buckley, Effect of Cathodic and Anodic Treatments of Carbon on the Electrode Kinetics of $\text{V}^{\text{IV}}/\text{V}^{\text{V}}$ Oxidation-Reduction, *J. Electrochem. Soc.*, 162, (2015) A1547-A1555.
- [28] D. Dixon, D.J. Babu, J. Langner, M. Bruns, L. Pfaffmann, A. Bhaskar, J.J. Schneider, F. Scheiba, H. Ehrenberg, Effect of oxygen plasma treatment on the electrochemical performance of the rayon and polyacrylonitrile based carbon felt for the vanadium redox flow battery application, *J. Power Sources*, 332, (2016) 240-248.
- [29] Q.H. Liu, G.M. Grim, A.B. Papandrew, A. Turhan, T.A. Zawodzinski, M.M. Mench, High Performance Vanadium Redox Flow Batteries with Optimized Electrode Configuration and Membrane Selection, *J. Electrochem. Soc.*, 159, (2012) A1246-A1252.
- [30] A.M. Pezeshki, J.T. Clement, G.M Veith, T.A. Zawodzinski, M.M Mench, High performance electrodes in vanadium redox flow batteries through oxygen-enriched thermal activation, *J. Power Sources*, 294, (2015) 333-338.
- [31] H. Fink, J. Friedl, U. Stimming, Composition of the Electrode Determines Which Half-Cell's Rate Constant is Higher in a Vanadium Flow Battery, *J. Phys. Chem. C.*, 120, (2016) 15893-15901.
- [32] M.A. Miller, A. Bourke, N. Quill, J.S. Wainright, R.P. Lynch, D.N. Buckley, R.F. Savinell, Kinetic Study of Electrochemical Treatment of Carbon Fiber Microelectrodes Leading to In Situ Enhancement of Vanadium Flow Battery Efficiency, *J. Electrochem. Soc.*, 163, (2016) A2095-A2102.
- [33] A.M Pezeshki, R.L Sacci, G.M. Veith, T.A. Zawodzinski, M.M. Mench, The Cell-in-Series Method: A Technique for Accelerated Electrode Degradation in Redox Flow Batteries, *J. Electrochem. Soc.*, 163, (2015) A5202-A5210.
- [34] I. Derr, M. Bruns, J. Langner, A. Fetyan, J. Melke, C. Roth, Degradation of all-vanadium redox flow batteries (VRFB) investigated by electrochemical impedance and X-ray photoelectron spectroscopy: Part 2 electrochemical degradation, *J. Power Sources*, 325, (2016) 351-359.

- [35] H. Liu, L. Yang, Q. Xu, C. Yan, Corrosion behavior of a bipolar plate of carbon–polythene composite in a vanadium redox flow battery, *RSC Adv.*, 5, (2015) 5928-5932.
- [36] B. Satola, L. Komsijska, G. Wittstock, Corrosion of Graphite-Polypropylene Current Collectors during Overcharging in Negative and Positive Vanadium Redox Flow Battery Half-Cell Electrolytes, *J. Electrochem. Soc.*, 165, (2018) A963-A969.
- [37] C. Jeppesen, S.S. Araya, S.L. Sahlin, S.J. Andreasen, S. Kær, An EIS alternative for impedance measurement of a high temperature PEM fuel cell stack based on current pulse injection, *Int. J. of Hydrogen Energy*, 42, (2017) 15851-15860.
- [38] H.J. Lee, S. Park, H. Kim, Analysis of the Effect of MnO₂ Precipitation on the Performance of a Vanadium/Manganese Redox Flow Battery, *J. Electrochem. Soc.*, 165, (2018) A952-A956.
- [39] M. C. Tucker, A. Weiss, A.Z. Weber, Improvement and analysis of the hydrogen-cerium redox flow cell, *J. Power Sources*, 327, (2016) 591-598.
- [40] V. Viswanathan, A. Crawford, D. Stephenson, S.W. Kim, W. Wang, B. Li, G. Coffey, E. Thomsen, G. Graff, P. Balducci, M. Kintner-Meyer, Vincent Sprenkle, Cost and performance model for redox flow batteries, *J. Power Sources*, 247, (2014) 1040-1051.

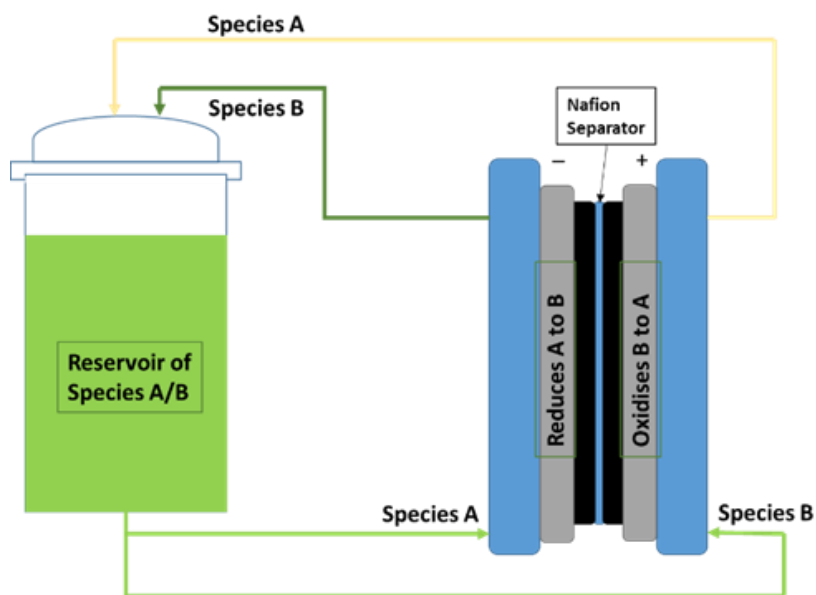


Fig 1 Schematic of symmetrical cell design for either 3 or 6 cm² area. Positive and negative electrolyte species are fed from the same tank, where species A is reduced when the cell is polarized and species B is oxidized. The reservoir typically contains a 50:50 mix of species A and B.

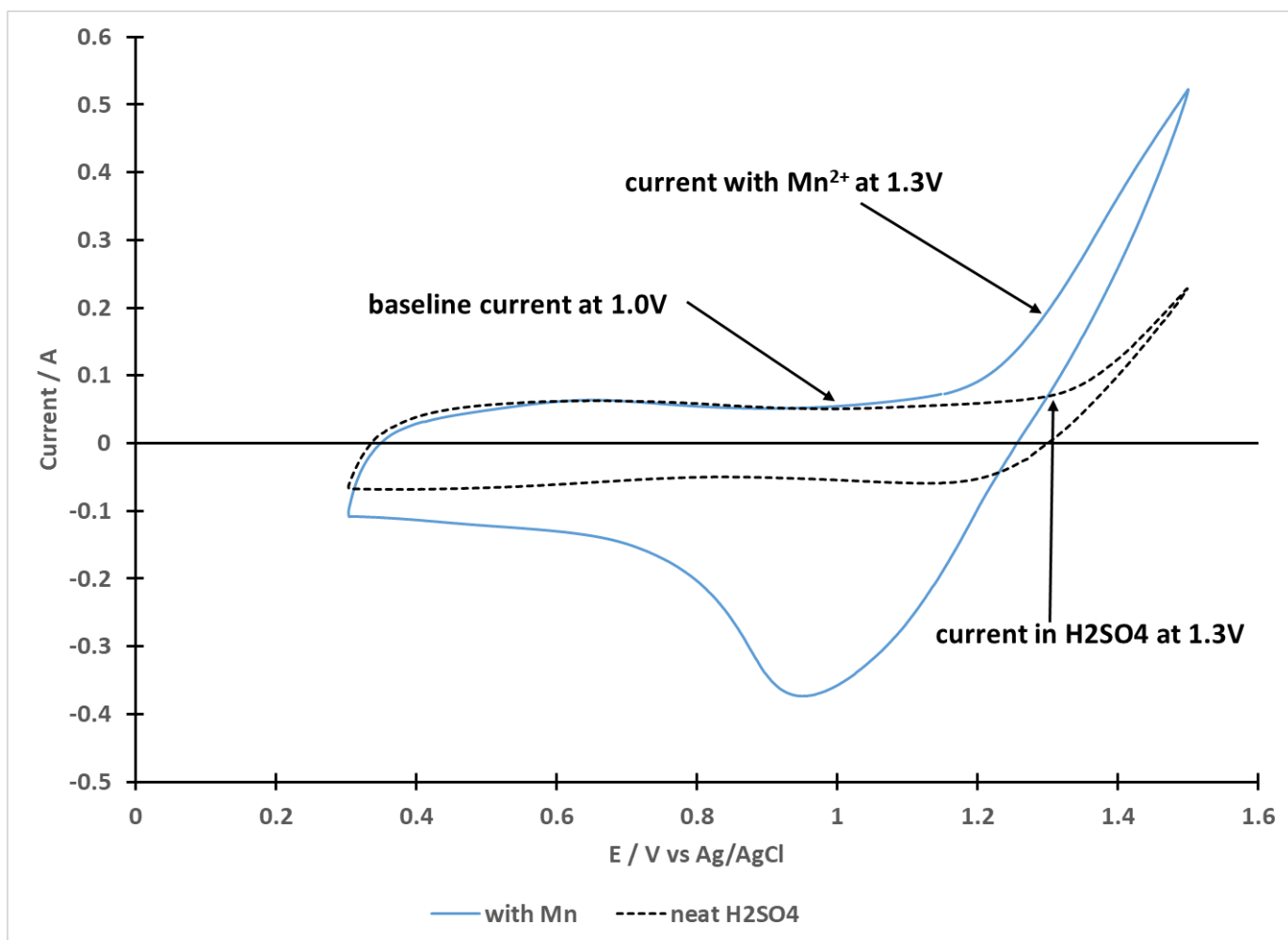


Fig. 2 Example of potentials and currents used to calculate coulombic efficiency during Mn oxidation on MMO and graphite electrodes.

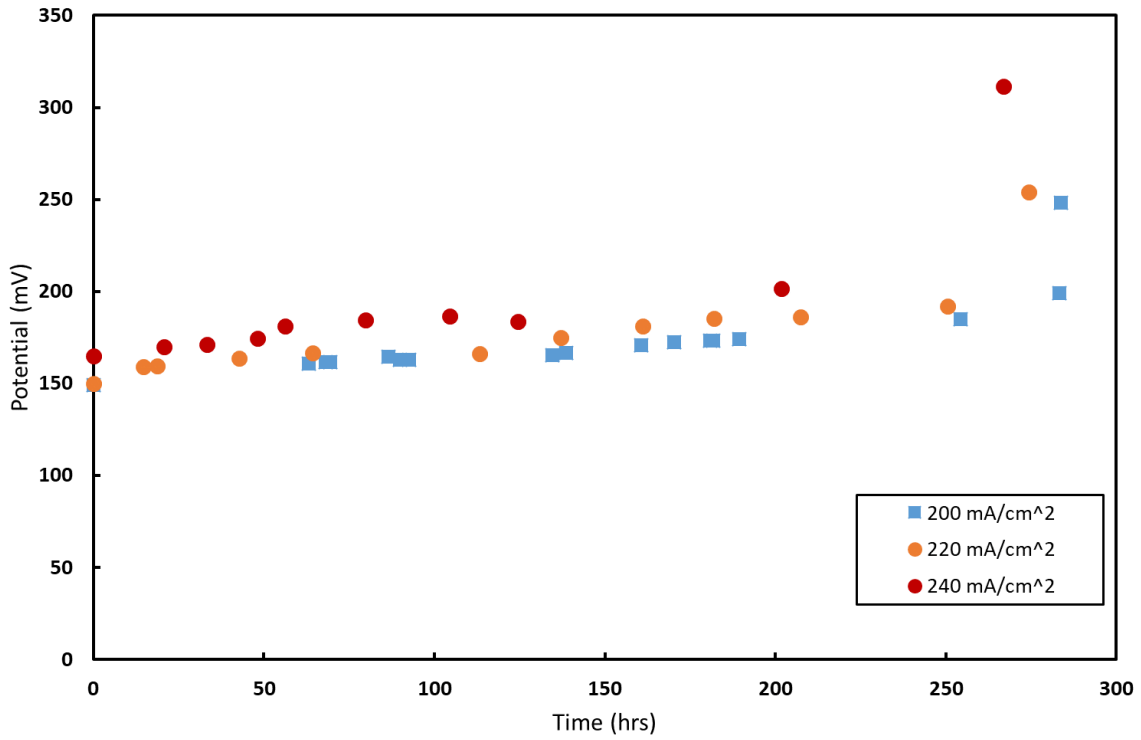


Fig 3 Plots of cell potential (mV) versus time (hrs) for three cells operating the $V^{3+/4+}$ redox couple galvanostatically at 200 mA/cm², 220 mA/cm² and 240 mA/cm² on graphitic felt carbon electrodes. Cell potential was noted to increase at 200-250 hrs in all three cases.

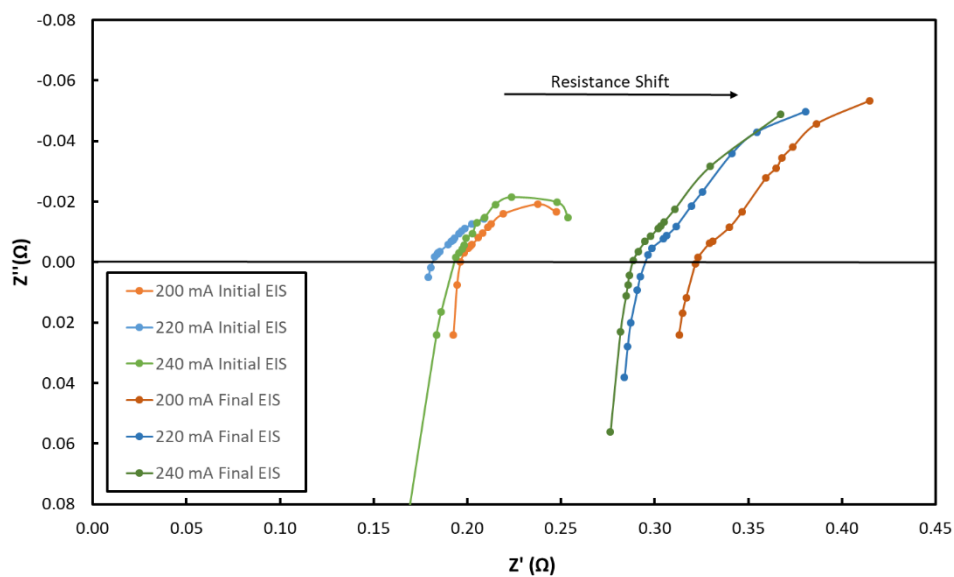


Fig 4 Nyquist plot for $V^{4+/5+}$ redox couple showing both the initial scan and the final scan for all three cells with graphitic carbon felt electrodes. Each cell was charged galvanostatically in between scans at 200, 220 and 240 mA/cm². A clear shift in both high frequency and charge transfer resistance is observed as indicated by the arrow inset.

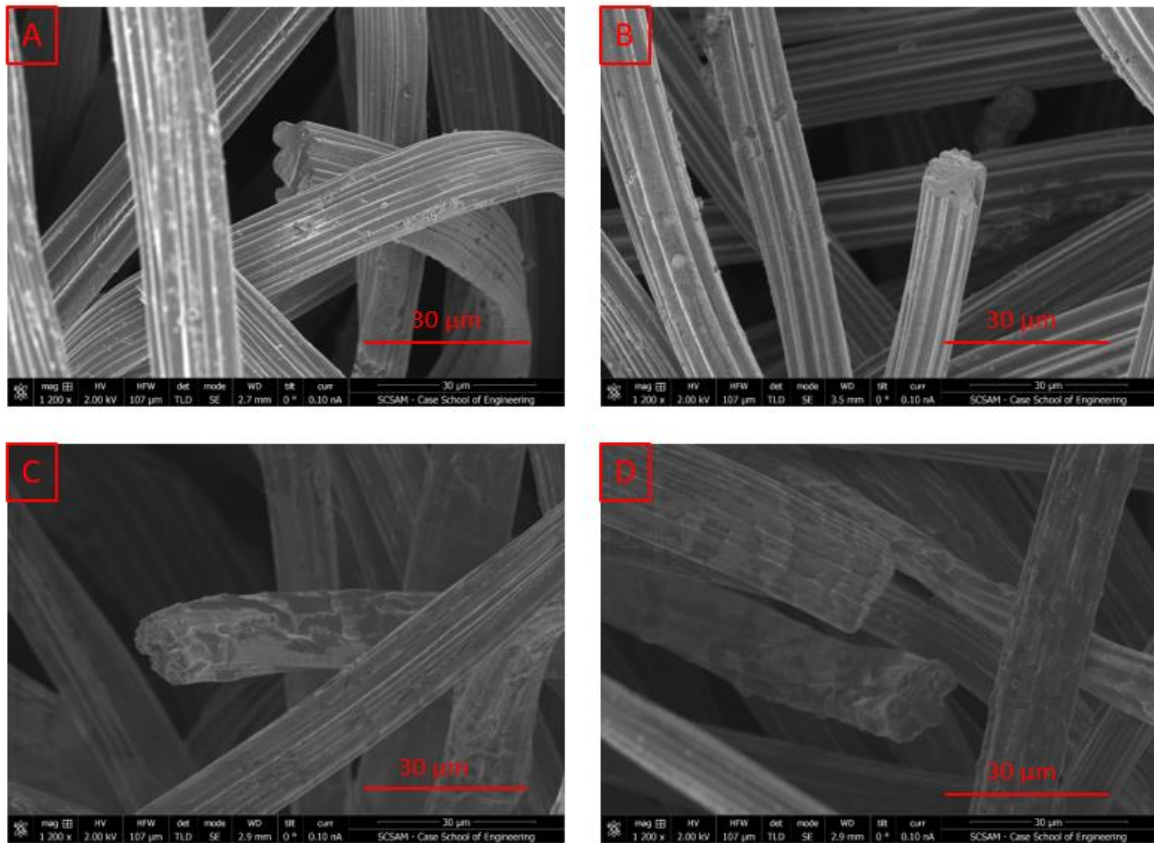


Fig 5 SEM micrographs of VDG carbon felt, with close-up views of heat treated carbon fibers (A) after heat treatment but prior to use in a cell, (B) after use in water mechanical test, (C) after use in V^4/V^5 cell as positive electrode, and (D) after use in V^4/V^5 cell as negative electrode. All samples are cut from the same roll of felt.

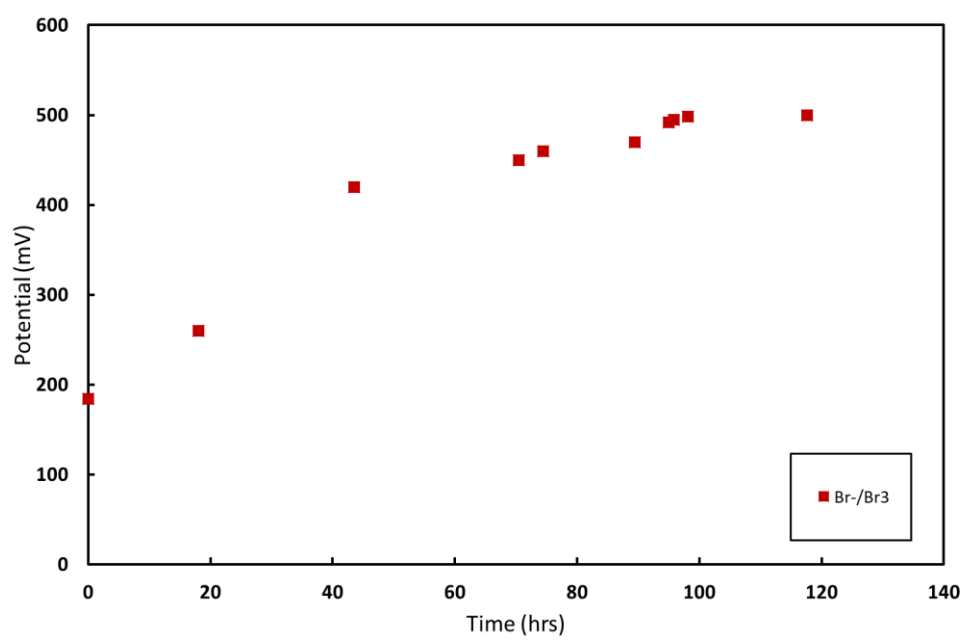


Fig 6 Polarization vs time for bromine redox cell with carbon felt electrodes. Applied current density 200 mA/cm^2 .

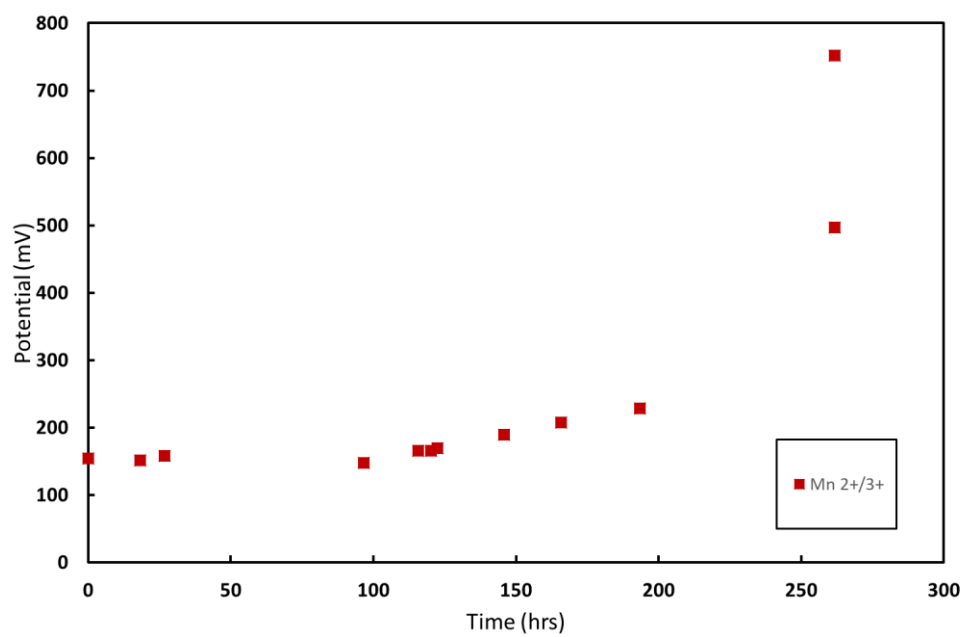


Fig 7 Polarization of the Mn/V cell at 43 mA/cm^2 , and carbon felt electrodes.

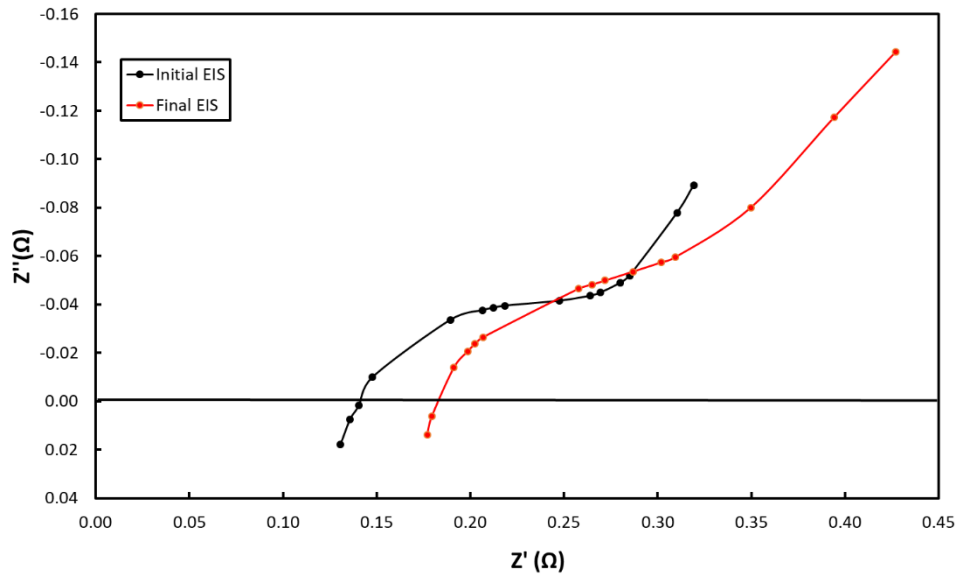


Fig 8 Nyquist plot for Mn/V cell showing both the initial and final scan for the same cell. The shift in the high frequency resistance from $\sim 0.14 \Omega$ to $\sim 0.19 \Omega$ shows an increase in contact resistance due to electrode degradation.

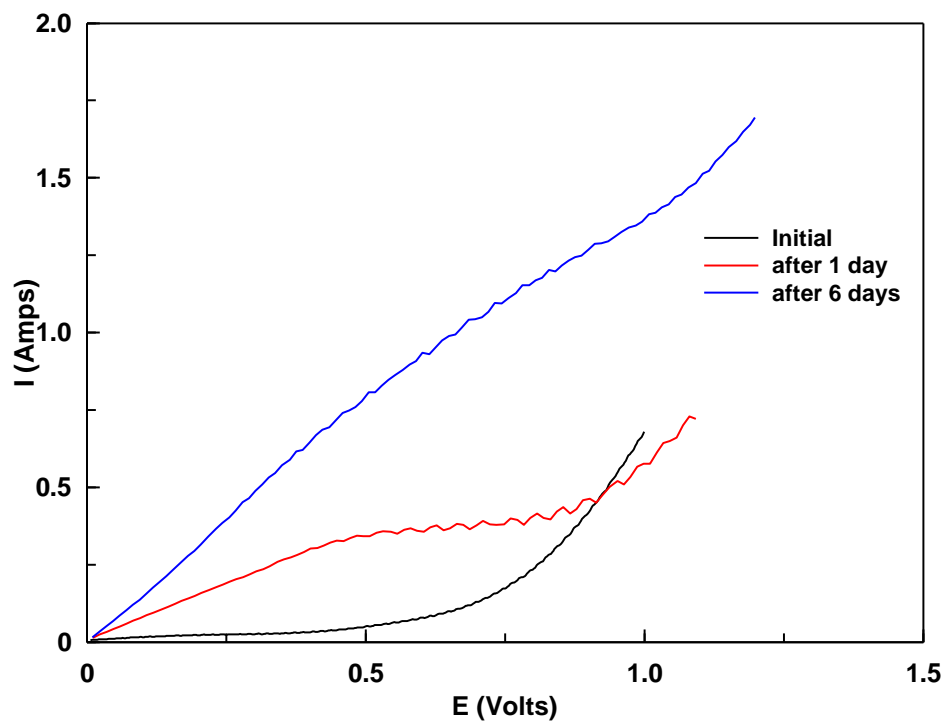


Fig 9 Polarization curves in Fe/Ce cell (1st trial). In between these curves, the cell potential was held at 1.05V.

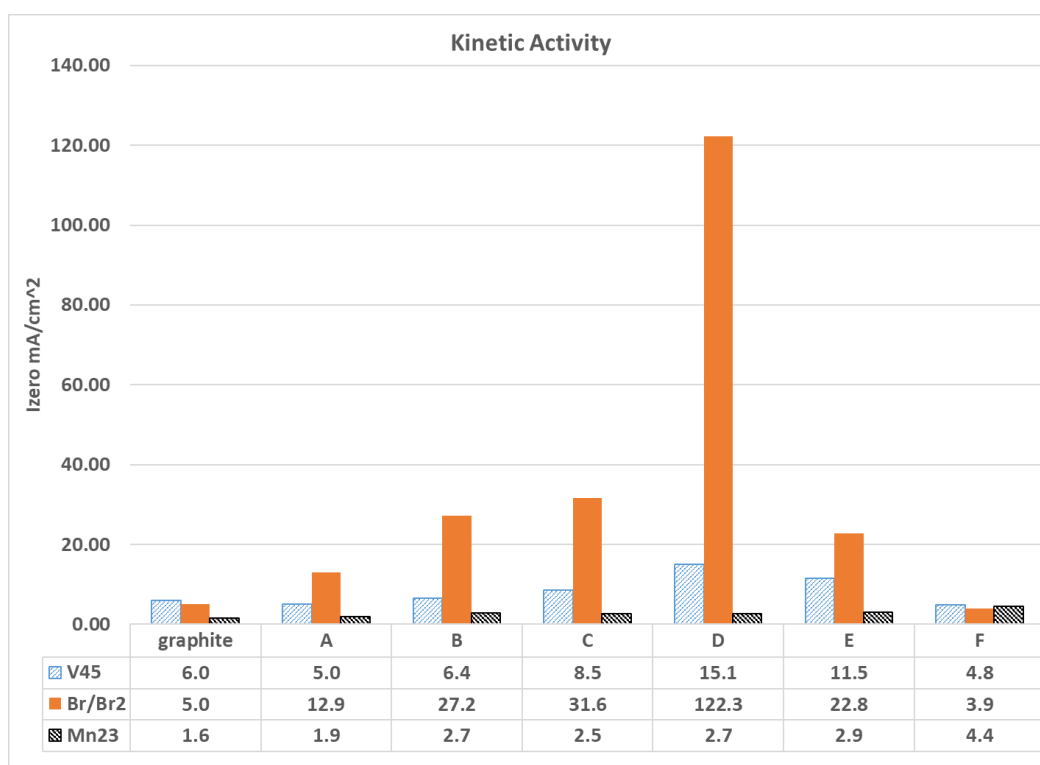


Fig 10 Kinetic activity for graphite and De Nora DSA® electrodes as measured by the apparent exchange current density for the vanadium, bromine and manganese redox couples. The exchange current density was calculated based on the geometric area of each electrode, not the total electrochemically active area.

Table 1 Summary of V^{4+/5+} trials

Duration of Battery Test (hrs)	Applied Current Density (mA/cm ²)	Cell Polarization Initial / final (mV)	Positive electrode weight change (% wt)	Negative electrode weight change (% wt)
283	200	149 to 248	7.4% loss	3.6% loss
274	220	150 to 254	4.8% loss	1.9% loss
267	240	165 to 311	3.6% loss	1.6% loss

Table 2 De Nora DSA® electrode components

Electrode	Components
A	Ir, Ru, Ti
B	Ru, Ti, Sn
C	Ru, Ti
D	Ir, Ru, Sn, Pt
E	Ir, Ta
F	Ir, Sn

Table 3 Coulombic efficiency (estimated) during Mn oxidation

Electrode	% of current going to O ₂ *
Graphite	2-5%
Carbon felt	5%
A	40 - 60%
B	10-15%
C	10-15%
D	40-50%
E	5%
F	50 - 70%

*- Ranges reflect the results of multiple trials.

Value given for carbon felt estimated from flow cell results shown above. All other values estimated from cyclic voltammetry on smooth electrodes.